SUPPORT VECTOR MACHINES FOR UNMIXING GEOLOGICAL MIXTURES

*Maitreya Mohan Sahoo, #Arun P.V., and *Alok Porwal

***Centre of Studies in Resources Engineering, Indian Institute of Technology Bombay, INDIA**
#Remote Sensing Laboratory, SIDEER, Ben-Gurion University of the Negev, ISRAEL

ABSTRACT

In this paper, we describe a Support Vector Machine (SVM) based approach for spectral unmixing of intimate geological mixtures. In this approach, we use the spectral distance of a pixel from the bounding hyperplane for a given endmember as a measure of purity of the pixel with respect to that specific endmember. The approach is implemented by first identifying the pure pixels in the image using various algorithms for estimating pixel purity, and then using spectral similarity measures to identify the endmembers. The pure pixels are then used to train a series of SVMs for all endmembers using the "one-against-all" approach. The trained SVMs are then used to process all pixels, and the spectral distance of each pixel from the bounding hyperplane for all endmembers are estimated. The approach is demonstrated using a simulated and real-world hyperspectral data. The results indicate that our approach outperforms linear and bilinear spectral unmixing approaches.

Index Terms— Spectral unmixing, SVM, pure pixels, spectral distance.

1. INTRODUCTION

Unmixing of the pixel spectra of hyperspectral images is a challenging inversion problem, particularly in the case of geological materials because of nonlinear mixing of endmembers. Intimate mixing on spatial scales smaller than the wavelength of incident photons, results in multiple interaction of one photon with more than one endmember[1]. Applying linear unmixing models to such complex mixtures leads to inaccurate abundance estimation[2]. Unmixing techniques such as hierarchical Bayesian estimation[3], block-coordinate descent algorithm for NMF minimization problems[4], and gradient descent algorithm[5] are iteration based and require some prior parameter assumptions for modeling. Sparse unmixing techniques[6] works well mostly for linearly mixed images; they also suffers from the drawback of highly correlated spectral signatures in the library which over-assigns the number of endmembers present in an image. Geometry based approaches such as the simplex projection technique[7] considers only a single spectra for a pure endmember and does not take endmember variability into account. Further, noisy pixels can lie exterior to the simplex, and the approximate projection works well only for linearly mixed pixels[8]. More recently, machine learning algorithms, both supervised and unsupervised, have been applied to spectral unmixing by several workers. Hopfield Neural Network has been successfully used for unmixing nonlinearly mixed images[9]. Kernel ridge regression[10] unmixes by mapping a nonlinear spectrum to a linear one using kernel functions. Deep learning architectures such as the convolutional neural networks (CNNs)[11] learn the feature maps at each convolution stage and perform comparable sub-pixel mapping. However, most of the supervised machine learning approaches including deep learning techniques require training samples which are practically difficult for real-world data sets.

In this paper, support vector machine is used as a machine learning tool to spectrally unmix geological mixtures. Being a robust tool, SVMs have the capability to learn features using a smaller number of training samples[12]. The main objective of an SVM is to segregate the feature space of a classified dataset using a discriminative hyperplane, also known as a decision surface. This research employs an approach using SVM classifier to unmix simulated mixtures (linearly and nonlinearly mixed), and remotely sensed geological datasets. The unmixing accuracy of the proposed approach with respect to prominent base-line unmixing approaches is evaluated using available ground truth. Since most of the geological materials can be distinguished by spectral features along narrow wavelength ranges, our proposed approach uses a subspace from the original feature space, therefore enhancing computational efficiency by feature pruning. Further reduction in feature dimensionality is achieved using transformations like principal component analysis (PCA) or maximum noise fraction (MNF). It also addresses the spectral variability among endmember spectral samples used for training SVM. Performance of this model is evaluated using various types of non-linearities and realworld datasets by comparing with some of the common unmixing methods and assessing its accuracy with known ground truth data.

2. METHODOLOGY

Given a hyperspectral image with no prior information about its endmember composition or their abundances. The spectral unmixing approach proposed in this research is summarized in Figure 1. A spectral subset of the image diagnostic of absorption features is chosen and preprocessed by applying dimensionality reduction algorithms (e.g., PCA/MNF) [13] in order to limit the number of endmembers and also to reduce noise in the image. The next step is to extract pure pixels from the image as they are representatives of the endmembers that are present with little or no mixing. In this regard, the pixel spectra are projected to convex hull based latent space to determine the image end members which are further identified by comparing them with a spectral library.

Once, the endmembers are identified, a series of SVM models are trained using the pure pixels of the image endmembers with a "one-against-all" approach. It may be noted that to increase the number of training samples, the pixels which are spectrally very close to image endmembers are also considered for training the SVM. These trained SVMs are then used to process all pixels, and the spectral distance of each pixel from the bounding hyperplane for all endmembers are estimated. For an SVM, the distance from the hyperplane is proportional to its functional value, which is expressed as:

$$Distance \propto g(x_i) = w.x_i + b$$

where x_i is the feature vector, w is the weight vector associated with each feature and b is the bias term. For simplicity, a spectral subset of the hyperspectral data cube is selected followed by transformation to a reduced dimension space using MNF transform.

3. EXPERIMENTS

For our experiment on assessing the performance of unmixing simulated and real datasets, a subset of real dataset's endmembers was used for generating simulated images and training the SVM. The AVIRIS scene of Cuprite

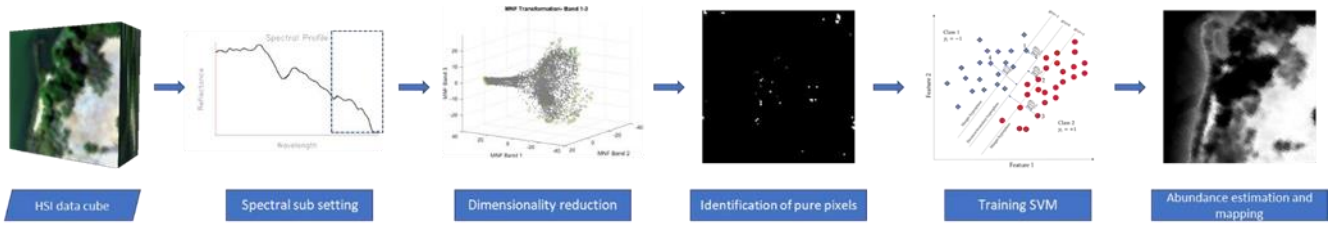

Figure 1: Flowchart of our proposed methodology

Hills, Nevada, which is considered to be a benchmark dataset for hyperspectral image analysis, was chosen for testing the algorithm with real-world dataset. The Cuprite Hills area has been well mapped and sampled. The samples have been extensively studied using laboratory spectroscopy. It comprises of exposed zones of advanced argillic alteration, along with silicified and opalized zones[14]. The key mineral assemblages include (1) Fe-bearing minerals (e.g., chlorite, goethite, hematite, jarosite, etc.) which show characteristic spectral absorption features centered at 1µm due to crystal field electronic transition; and (2) phyllosilicates minerals (e.g., alunite, buddingtonite, kaolinite, muscovite, etc.) which have various absorption features between 2.0-2.5 µm due to molecular vibration of metal-OH bond.

For our simulation dataset, we selected three endmembers, namely, Alunite, Buddingtonite, and Chalcedony. Further, we selected three for real dataset- Alunite, Chalcedony and Na-Montmorillonite endmembers from the Nevada data. Spectral absorption features of these minerals are tabulated in Table 1.

Endmember	Spectral absorption features (2.0 – 2.5 µm region)
Alunite $KAl_3(SO_4)_2(OH)_6$	• 2.16 – 2.22 µm (Al-OH vibration)
Buddingtonite $NH_4AlSi_3O_8 .0.5H_2O$	• 2.02, 2.12 µm (NH_4 vibration) • 2.16 – 2.22 µm (Al-OH vibration)
Chalcedony SiO_2	No absorption feature (Presence of metal-OH impurities give some absorption)
Na-Montmorillonite $Na_{0.33}(Al,Mg)_2(Si_4O_{10})(OH)_2 \cdot nH_2O$	• 2.16 – 2.22 µm (Al-OH vibration) • 2.30-2.36 µm (Mg-OH vibration)

Table 1: Endmembers selected for implementing our proposed unmixing model with their spectral absorption features in the SWIR region (2.0 – 2.5 µm)

3.1. Simulated dataset

Synthetic images were generated by mixing the random abundances of the endmembers that were derived using spherical gaussian distribution (Figure 2). The spectra of the endmembers comprising 48 bands in the SWIR region, were

mixed linearly and also by using four different nonlinear mixing models- Fan model[15], GBM[5], PPNMM[3] (having positive and negative nonlinearity parameters), and MLM with the mixing parameters used by Heylen and Scheunders, 2016[16].

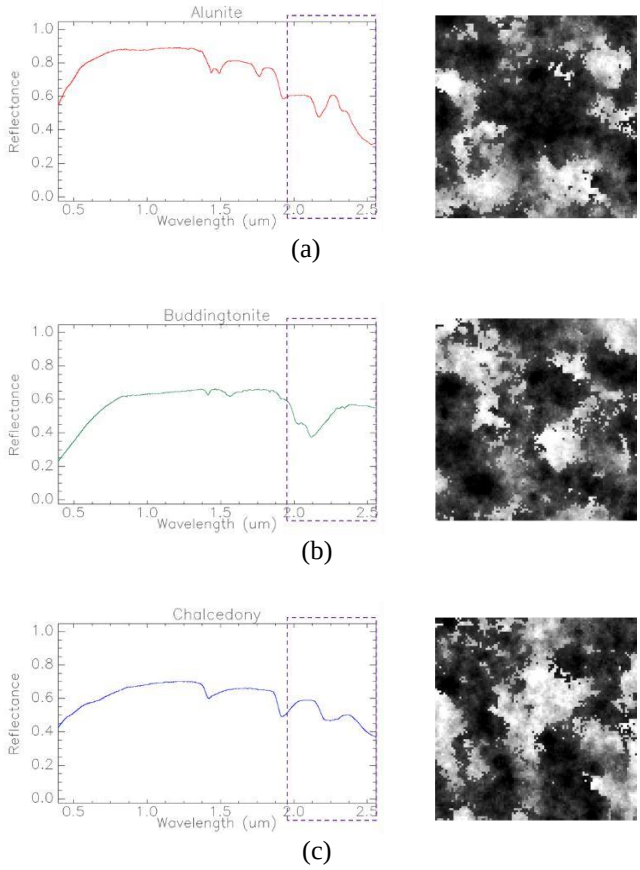

Figure 2: Spectra of selected endmembers obtained from USGS spectral library with spectral subset in the SWIR region (2.0 – 2.5 µm) and generated abundances for (a) Alunite, (b) Buddingtonite, (c) Chalcedony

Two sets of images were created; one without noise, and the other with added independent and identically distributed white gaussian noise of SNR 20. The dimensions of the simulated images are 100 by 100 pixels and 48 bands.

These datasets were unmixed using the proposed SVM-based model and the results were compared with the results obtained by linear and bilinear unmixing models.

The performance of the unmixing models were assessed using two performance metrics, namely, mean abundance error (MAE) with their standard deviation (Table 2) and root mean squared error (RMSE) (Table 3).

The results show that, as compared to the linear and bilinear unmixing models, the SVM-based unmixing model performs better with the synthetic images, both without and with noise. The fully constrained linear unmixing model works better only for the linearly mixed images; however, for the non-linearly mixed images, it gives error values as high as 0.17 (Table 3).

Using the SVM based approach for unmixing images without noise, the highest MAE and RMSE was obtained for the Fan model (0.12 and 0.15) followed by the GBM model (0.06 and 0.08). The bilinear unmixing performs better for these models as both these images were generated using bilinear mixing. However, for noisy images, the proposed SVM-based method outperforms bilinear unmixing. Figures 3 and 4 depict the bar plots showing the unmixing performances of the three methods.

	FCLU	**Bilinear**	**SVM based**
LMM	1.70E-09	2.05e-7 (1.95e-7)	6.67e-9 (4.88e-9)
Fan model	0.15776 (7%)	7.4e-7 (4.5e-7)	0.12313 (9%)
GBM	0.1292 (7%)	4.5e-7 (3.62e-7)	0.06634 (6%)
PPNMM1	0.13894 (8%)	0.03475 (3%)	0.00609 (0.3%)
PPNMM2	0.07986 (7%)	0.03538 (3%)	0.00998 (0.5%)
MLM	0.09711 (8%)	0.08181 (8%)	0.03486 (4%)

(A)

	FCLU	**Bilinear**	**SVM based**
LMM	2.40E-09	0.17335 (15%)	0.01467 (1%)
Fan model	0.15786 (8%)	0.17335 (15%)	0.08328 (8%)
GBM	0.12941 (7%)	0.17335 (15%)	0.02752 (2%)
PPNMM1	0.13911 (8%)	0.16984 (14%)	0.01703 (1%)
PPNMM2	0.08219 (7%)	0.18288 (16%)	0.02012 (2%)
MLM	0.09854 (8%)	0.17903 (14%)	0.04016 (3%)

(B)

Table 2: MAE obtained for unmixing images: (A) without noise, (B) with noise using linear, bilinear and SVM-based unmixing

	FCLU	Bilinear	SVM based
LMM	3.53E-09	2.83E-07	8.27E-09
Fan model	0.17493	8.67E-07	0.15416
GBM	0.14615	5.78E-07	0.08757
PPNMM1	0.16123	0.04576	0.00681
PPNMM2	0.10664	0.04696	0.01111
MLM	0.12726	0.11182	0.05326

(A)

	FCLU	Bilinear	SVM based
LMM	6.30E-09	0.22746	0.01826
Fan model	0.17604	0.22746	0.11870
GBM	0.14762	0.22746	0.03269
PPNMM1	0.16198	0.21922	0.02066
PPNMM2	0.10866	0.24150	0.02532
MLM	0.12846	0.22974	0.05119

(B)

Table 3: RMSE obtained for unmixing images: (A) without noise, (B) with noise using linear, bilinear and SVM-based unmixing

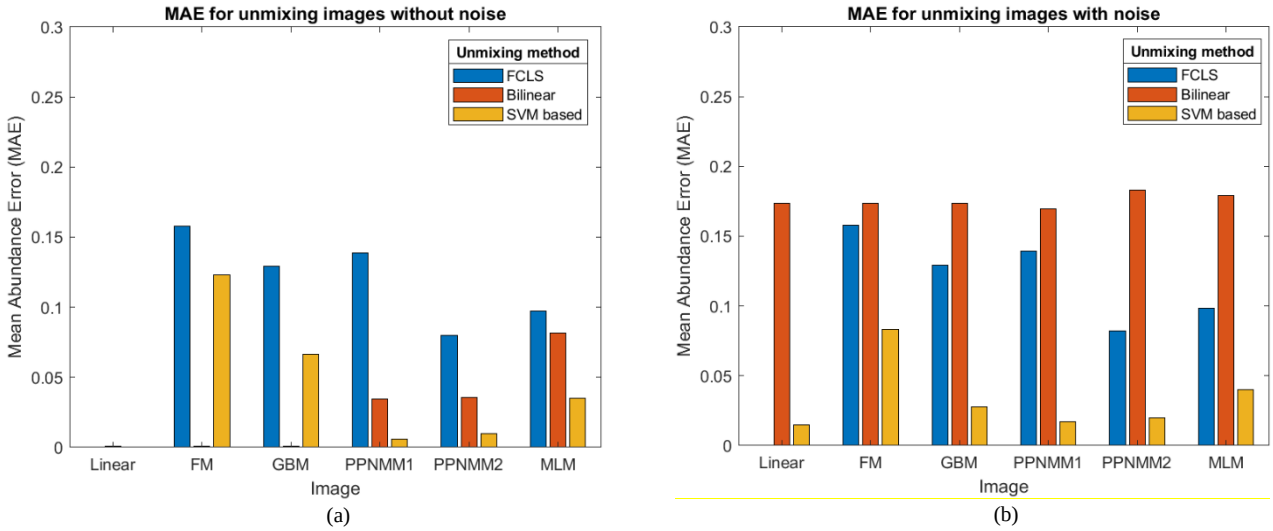

Figure 3: Bar plots showing mean abundance errors for unmixing linearly and nonlinearly mixed images using FCLS, Bilinear and SVM-based unmixing: (a) images without noise, (b) images with noise

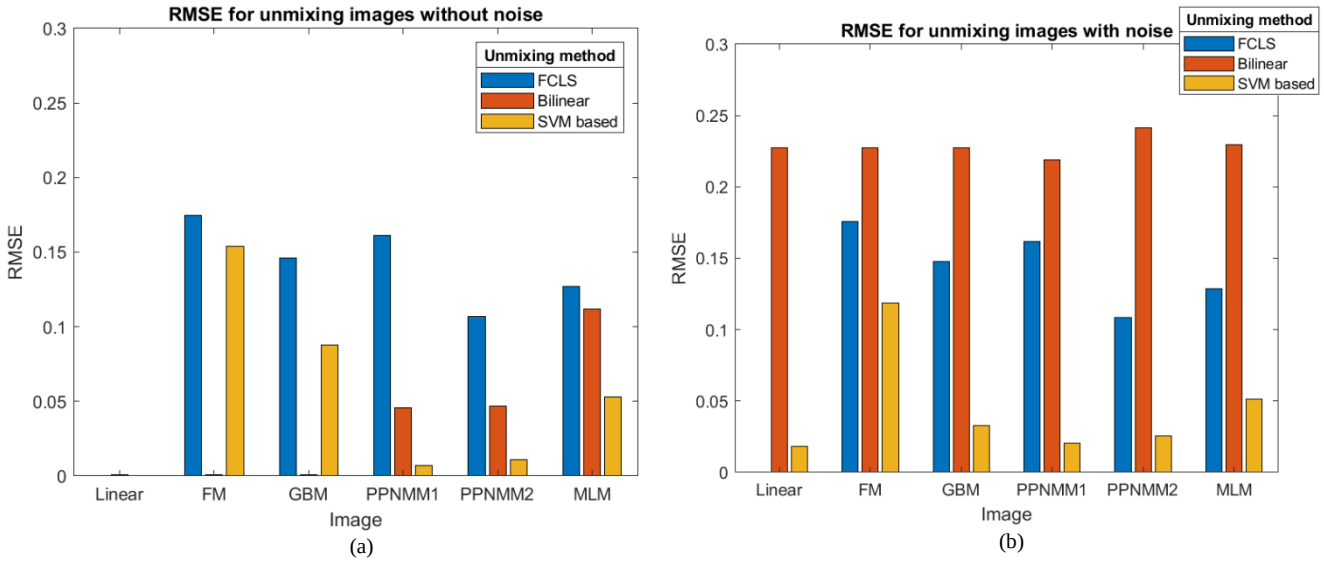

Figure 4: Bar plots showing RMSE for unmixing linearly and nonlinearly mixed images using FCLS, Bilinear and SVM-based unmixing: (a) images without noise, (b) images with noise

The plot also shows that the SVM based unmixing works well for the transformed dataset. Features transformation helps in two ways- (i) it improves identification of pure pixels, and (ii) it helps in improving the computational performance.

However, real images have larger endmember variability, aa well as noise. Also, it is likely to have endmember outliers. The above issues have to be addressed for proper training of the SVM models. Obtaining representative samples of the endmembers directly from an image does not require any assumption related to the statistical distribution of their spectra. This further eliminates variations which are not physically meaningful[17]. However, the accuracy of unmixing would also depend on the number of pure pixels samples selected for an endmember class and their relative location in the transformed feature space. Sample points which are clustered and spaced closely are more likely to be representatives of endmember pure pixels.

The above issues have been dealt with in the unmixing of real dataset.

3.2. Real dataset

A subset of the AVIRIS reflectance data for Cuprite Hills, Nevada, comprising 750 by 614 pixels and 224 bands was used for testing the algorithm using real dataset. Bands 12, 105-115, 150-170 and 223-224 were removed because of water-vapor absorption and low SNR. Of the remaining bands, bands 175-222 corresponding to 2-2.5 µm (shortwave infrared region) were chosen for modelling, because the diagnostic absorption features related to Metal - OH vibrations lie within this range.

The pure pixels belonging to Alunite, Chalcedony and Na-Montmorillonite were selected based on their diagnostic absorption features as previously listed.

Three SVM models were trained using pure pixels of each of the three endmember mineral species. All pixels of the image were then processed using the trained SVM and the relative abundance of each of the three minerals were estimated for each pixel based on the distance to the bounding hyperplane as described above in Section 2. The above unmixing results,

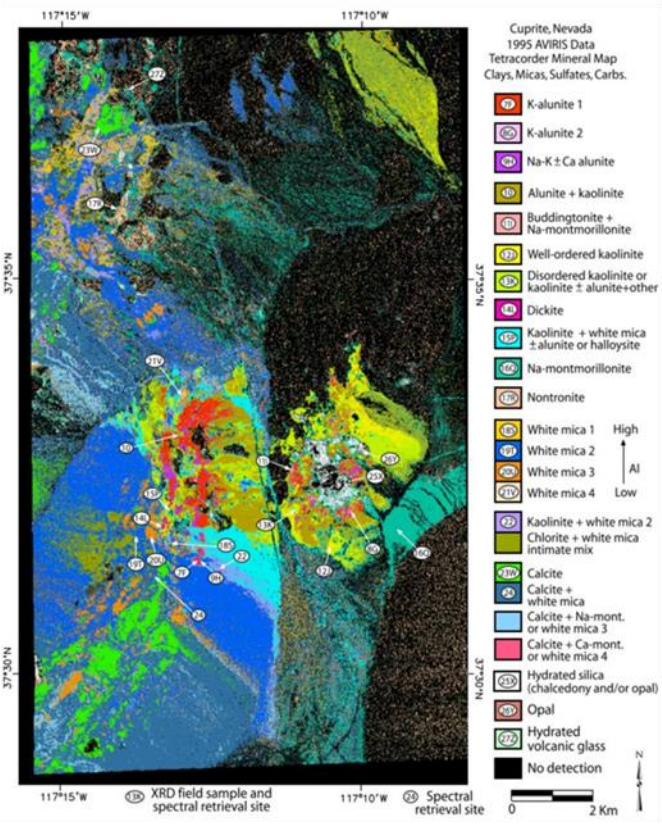

Figure 5: USGS Tetracorder map showing the location of different mineral endmembers in the Cuprite region, Nevada (adopted from Swayze et. al., 2014)

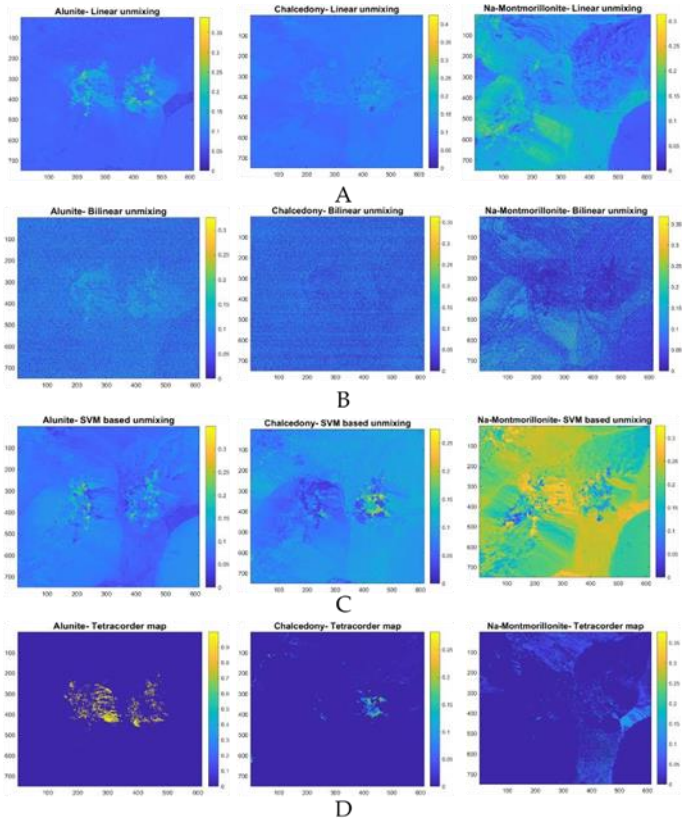

Figure 6: Fractional abundance estimations obtained for selected endmembers using (A) linear unmixing, (B) bilinear unmixing, and (C) proposed SVM based unmixing. (D) shows the Tetracorder abundance mapping of these endmembers (scaled from 0 to 1)

as well as those obtained using linear and bilinear unmixing, were compared with the results obtained using Tetracorder. Since there is limited ground truth abundance information available for all pixels, the estimated abundance maps (Figures 6- (A), (B) and (C)) were visually compared with the published Tetracorder map (Figure 5) and its results scaled from 0 to 1 (Figure 6-(D)). Pixels common to Tetracorder classification results and the abundance images obtained using the proposed method were visually compared. Qualitative assessment of our proposed unmixing model by visual comparison with the available literatures[6],[18],[19] also provided consistency with the results.

4. CONCLUSION

Our proposed method of spectral unmixing using SVM-based approach worked well for both simulated and real datasets. The performance metrics used for evaluating the unmixing of synthetic images were MAE and RMSE, and the unmixing results for real-world dataset was visually compared with the Tetracorder results and available literatures for a qualitative assessment. Our developed unmixing model only requires pure pixels for training, which are sparsely available in any image dataset; this helps in better computational performance with comparable results produced by other unmixing techniques. SVM model also has an added advantage of accommodating spectral variations of representative samples of endmembers during training; it helps to minimize the unmixing errors.

Future scope in developing this model includes training datasets with wider variability. Improving the performance of the SVM-based unmixing model using fuzzy membership values would also help in accurate abundance mapping by training a minimal number of mixed pixels. Implementing this model to study its performance on images of varying noise levels, endmember compositions, mixing models, abundance distributions and feature transformations will be discussed further in a greater detail.

5. REFERENCES

[1] Keshava, N. and Mustard, J.F., 2002. Spectral unmixing. IEEE signal processing magazine, 19(1), pp.44-57.

[2] Jia, X., Dey, C., Fraser, D., Lymburner, L. and Lewis, A., 2010, June. Controlled spectral unmixing using extended support vector machines. In 2010 2nd Workshop on Hyperspectral Image and Signal Processing: Evolution in Remote Sensing (pp. 1-4). IEEE.

[3] Altmann, Y., Halimi, A., Dobigeon, N. and Tourneret, J.Y., 2012. Supervised nonlinear spectral unmixing using a postnonlinear mixing model for hyperspectral imagery. IEEE Transactions on Image Processing, 21(6), pp.3017-3025.

[4] Févotte, C. and Dobigeon, N., 2015. Nonlinear hyperspectral unmixing with robust nonnegative matrix factorization. IEEE Transactions on Image Processing, 24(12), pp.4810-4819.

[5] Halimi, A., Altmann, Y., Dobigeon, N. and Tourneret, J.Y., 2011. Nonlinear unmixing of hyperspectral images using a generalized bilinear model. IEEE Transactions on Geoscience and Remote Sensing, 49(11), pp.4153-4162.

[6] Iordache, M.D., Bioucas-Dias, J.M. and Plaza, A., 2011. Sparse unmixing of hyperspectral data. IEEE Transactions on Geoscience and Remote Sensing, 49(6), pp.2014-2039.

[7] Heylen, R., Burazerovic, D. and Scheunders, P., 2011. Fully constrained least squares spectral unmixing by simplex projection. IEEE Transactions on Geoscience and Remote Sensing, 49(11), pp.4112-4122.

[8] Pu, H., Xia, W., Wang, B. and Jiang, G.M., 2013. A fully constrained linear spectral unmixing algorithm based on distance geometry. IEEE transactions on geoscience and remote sensing, 52(2), pp.1157-1176.

[9] Li, J., Li, X., Huang, B. and Zhao, L., 2016. Hopfield neural network approach for supervised nonlinear spectral unmixing. IEEE Geoscience and Remote Sensing Letters, 13(7), pp.1002-1006.

[10] Koirala, B., Khodadadzadeh, M., Contreras, C., Zahiri, Z., Gloaguen, R. and Scheunders, P., 2019. A supervised method for nonlinear hyperspectral unmixing. Remote Sensing, 11(20), p.2458.

[11] Arun, P.V., Buddhiraju, K.M. and Porwal, A., 2018. CNN based sub-pixel mapping for hyperspectral images. Neurocomputing, 311, pp.51-64.

[12] Brown, M., Lewis, H.G. and Gunn, S.R., 2000. Linear spectral mixture models and support vector machines for remote sensing. IEEE Transactions on geoscience and remote sensing, 38(5), pp.2346-2360.

[13] Bioucas-Dias, J.M., Plaza, A., Dobigeon, N., Parente, M., Du, Q., Gader, P. and Chanussot, J., 2012. Hyperspectral unmixing overview: Geometrical, statistical, and sparse regression-based approaches. IEEE journal of selected topics in applied earth observations and remote sensing, 5(2), pp.354-379.

[14] Swayze, G.A., Clark, R.N., Goetz, A.F., Livo, K.E., Breit, G.N., Kruse, F.A., Sutley, S.J., Snee, L.W., Lowers, H.A., Post, J.L. and Stoffregen, R.E., 2014. Mapping advanced argillic alteration at Cuprite, Nevada, using imaging spectroscopy. Economic Geology, 109(5), pp.1179-1221.

[15] Fan, W., Hu, B., Miller, J. and Li, M., 2009. Comparative study between a new nonlinear model and common linear model for analysing laboratory simulated-forest hyperspectral data. International Journal of Remote Sensing, 30(11), pp.2951-2962.

[16] Heylen, R. and Scheunders, P., 2015. A multilinear mixing model for nonlinear spectral unmixing. IEEE transactions on geoscience and remote sensing, 54(1), pp.240-251.

[17] Zare, A. and Ho, K.C., 2013. Endmember variability in hyperspectral analysis: Addressing spectral variability during spectral unmixing. IEEE Signal Processing Magazine, 31(1), pp.95-104.

[18] Iordache, M.D., Bioucas-Dias, J.M. and Plaza, A., 2012. Total variation spatial regularization for sparse hyperspectral unmixing. IEEE Transactions on Geoscience and Remote Sensing, 50(11), pp.4484-4502.

[19] Borsoi, R.A., Imbiriba, T., Bermudez, J.C.M. and Richard, C., 2020. A blind multiscale spatial regularization framework for kernel-based spectral unmixing. IEEE Transactions on Image Processing, 29, pp.4965-4979.